Chapter K

The 1992 Little Skull Mountain Earthquake Sequence, Southern Nevada Test Site

By Kenneth D. Smith,[1] James N. Brune,[1] Diane dePolo,[1] Martha K. Savage,[1] Rasool Anooshehpoor,[1] *and* Anne F. Sheehan[2]

Contents

Figures

[1]University of Nevada-Reno Seismological Laboratory, Reno, Nev.
[2]Cooperative Institute for Research in Environmental Sciences, University of Colorado, Boulder, Colo.

Tables

[For table of abbreviations and conversions, click here]

Abstract

The M_L 5.6–5.8 June 29, 1992, Little Skull Mountain, Nevada, earthquake occurred in the southwest portion of the Nevada Test Site approximately 20 kilometers from Yucca Mountain, a potential site for a high-level radioactive-waste repository. The earthquake involved predominantly down-to-the-southeast dip-slip fault motion with a small left-slip component on a steeply dipping 65°–70° northeast-striking fault. The mainshock originated near the base of the aftershock zone and ruptured up and to the northeast, and the mainshock rupture and the majority of the aftershock sequence were confined to depths between 6 and 12 kilometers. All three M_L 4+ aftershocks, the largest of the aftershock activity, occurred off the mainshock fault plane on secondary structures in the aftershock zone. The nearest strong-motion instrument, located 11 kilometers southwest of the epicenter, recorded a peak acceleration of 0.206 *g*. The earthquake occurred adjacent to the Rock Valley fault zone within an area of prior concentrated background seismicity and near the intersection of several northeast-striking faults in the southern Nevada Test Site on which Quaternary movement has taken place.

Introduction

The Little Skull Mountain (LSM) earthquake occurred on June 29, 1992 (origin time 101422.47 Universal Time (UT)) at lat 36°43.16′ N., long 116°17.76′ W., approximately 20 km southeast of a potential site for a high-level radioactive-waste repository at Yucca Mountain, Nev. (fig. 1). The event occurred at a depth of 11.8 km with M_L values of 5.8 and 5.6 as recorded by the University of Nevada-Reno Seismological Laboratory (UNRSL) and the National Earthquake Information Center of the U.S. Geological Survey (USGS), respectively.

In this study we develop an interpretation of the geometry of mainshock faulting and other active structures within the LSM aftershock zone from a set of high-quality earthquake locations and well-constrained short-period focal mechanisms. Several faults were involved in the aftershock sequence. The geometry of these structures is correlated, where possible, with mapped features in the south-central Nevada Test Site (NTS). Also, from the aftershock distribution, we establish constraints on the static stress drop and average displacement during mainshock faulting. Previous studies (Harmsen, 1994, and Meremonte and others, 1995) were limited to the early aftershock period, whereas we have used data through the end of 1992. Also, data from additional portable instrumentation are included in earthquake relocations. We have also applied a slightly different location procedure than used in previous studies and have attempted to isolate only the highest quality aftershock locations from a larger data set.

Our interpretation is that the earthquake involved down-to-the-southeast dip-slip motion, with a small component of left-slip, on a steeply dipping (≈65°–70°) northeast-striking fault. The mainshock originated at the base of the aftershock zone with rupture propagation up and to the northeast, and the mainshock fault surface, and almost the entire sequence, were confined to depths between 6 and 12 km. All three of the largest aftershocks ($M_L > 4$) took place not on the mainshock fault plane but rather on secondary structures within the aftershock zone. The closest strong-motion instrument, located 11 km southwest of the mainshock epicenter on a thick section of sediments at Lathrop Wells, Nev., recorded a peak ground acceleration of 0.206 *g*.

The LSM sequence provides one of the few visual images and "senses-of-motion" on subsurface structure in the region. Focal mechanisms have been calculated for earthquakes in the southern Great Basin since comprehensive seismic monitoring began in 1978. (See U.S. Geological Survey Open-File Reports for the Southern Great Basin Seismic Network; for example, Harmsen, 1993; Harmsen and Bufe, 1992.) However, these earthquakes have not been associated with extensive sequences, and the ambiguities in the actual fault-plane orientations still exist.

Several tectonic models have been proposed for the Yucca Mountain area in attempts to evaluate the seismic hazard from the surface expression of mapped Quaternary faults. Fridrich (1999) pointed out that several proposed kinematic models rely on buried structures with little physical evidence for their existence. Low-angle detachment faults extending through Jackass Flat and beneath Yucca Mountain have been invoked to account for the tilting and the close spacing of normal faults in the Yucca Mountain block (Scott, 1990). Large-scale regional strike-slip faulting extending through Crater Flat has been proposed to address mapped offsets in Paleozoic rocks (Schweichert, 1989).

Considering its proximity to Yucca Mountain and the ongoing seismic hazard evaluation for the potential repository site, the LSM sequence is significant in providing a wealth of seismicity and ground motion data. Harmsen (1994) and Meremonte and others (1995) have reported on several aspects of the LSM sequence. Harmsen (1994) inferred the regional

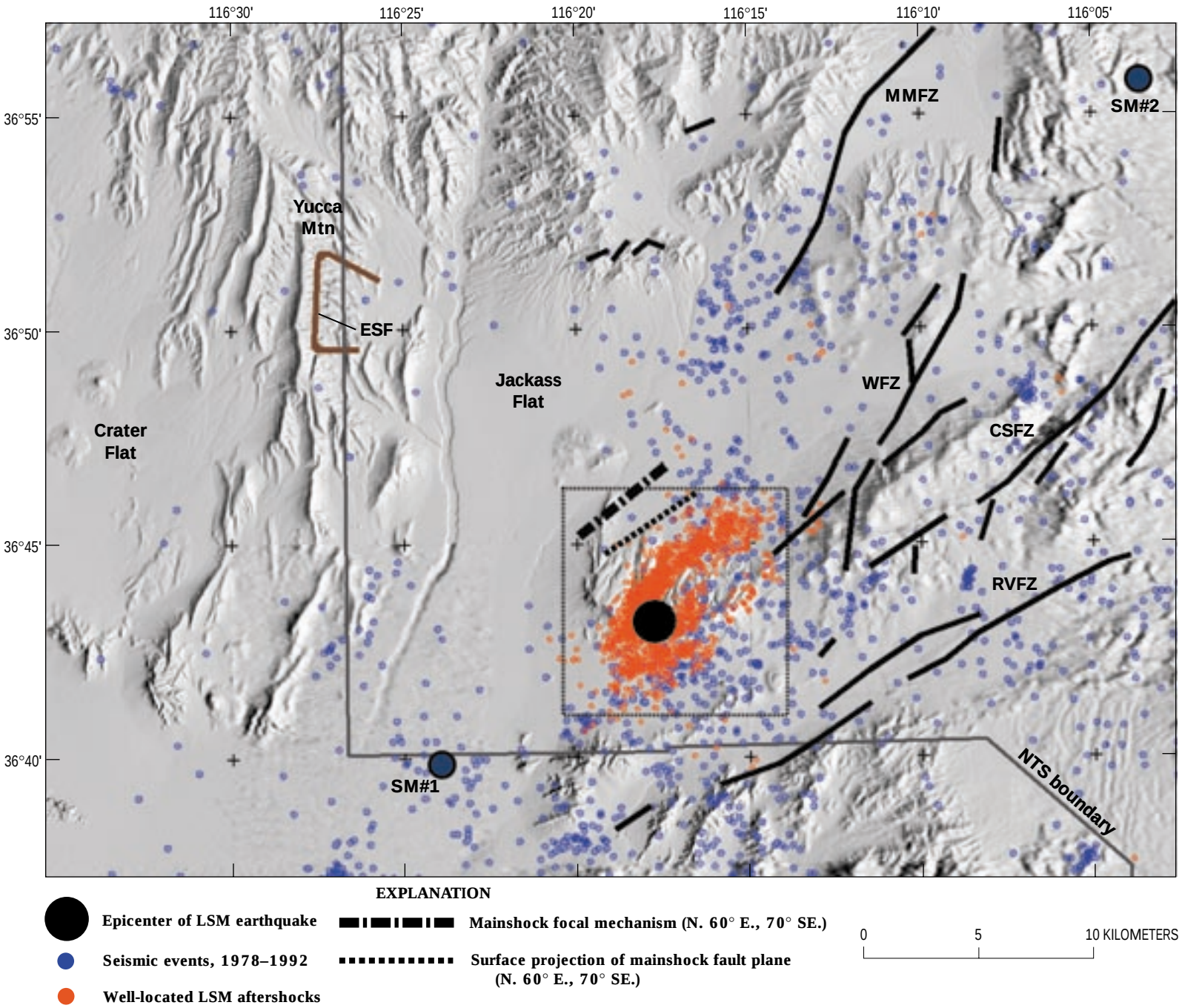

Figure 1. Shaded relief map of Little Skull Mountain and Yucca Mountain regions. Dotted rectangle, area of study, shown in other figures. Labeled fault zones: MMFZ, Mine Mountain; WFZ, Wahmonie; RVFZ, Rock Valley; CSFZ, Cane Spring. SM#1 and SM#2 are locations of strong-motion instruments. ESF, Exploratory Studies Facility.

stress directions and preferred fault planes within the aftershock zone from a set of short-period focal mechanisms and a stress inversion routine. Meremonte and others (1995) provided an interpretation of the geometry of faulting within the aftershock zone with respect to local mapped Quaternary faults using a limited set of "robust hypocentral determinations." They (Meremonte and others, 1995) also discussed the local geology and summarized some models of deformation in and around the LSM area.

The 1992 LSM earthquake is notable in several respects. It was the largest earthquake in the southern Great Basin since an M_L 5.7–6.1 earthquake near Caliente, Nev., in 1966 (Rogers and others, 1991; Meremonte and Rogers, 1987), and has been the largest earthquake within the Southern Great Basin Seismic Network (SGBSN) since comprehensive regional seismic monitoring began in 1978. It also has been the largest tectonic event within 50 km of Yucca Mountain in historical times. The May 1993, M_L 6.1 Eureka Valley, Calif., earthquake has been the largest of the most recent earthquakes in the southern Great Basin (Peltzer and Rosen, 1995). This event occurred at the west edge of the SGBSN in the Eastern California shear zone (Dokka and Travis, 1990). Other, more recent moderate-sized earthquakes in the southern Great Basin have included a series of M 5+ events near Ridgecrest, Calif., in the mid 1990's in southern Owens Valley (Hauksson and others, 1995).

The LSM event was the largest earthquake of an unprecedented pulse of seismicity that was recorded throughout the Basin and Range following the June 28, 1992 M_S 7.5 Landers, Calif., earthquake. The conclusion was that this unusual short-term increase in earthquake activity, as well as the LSM earthquake itself, was triggered by the Landers event (Hill and others, 1993; Anderson and others, 1993; Bodin and Gomberg, 1994; Gomberg and Bodin, 1994). Although the LSM earthquake took place 20 hours following Landers, earthquake activity in the LSM source region was detected within the coda of the Landers event, providing the best evidence for a direct triggering mechanism (Anderson and others, 1994; Gomberg and Bodin, 1994).

A mapped fault with Quaternary offsets that is closest to the epicenter of the LSM earthquake is the northeast-striking Rock Valley fault zone (RVFZ; fig. 1), although the LSM earthquake did not occur in the RVFZ. The RVFZ is adjacent to and south of LSM and extends in an east-northeast direction from the western Specter Range through the eastern part of the Nevada Test Site (NTS) (Carr, 1984, 1990; Scott, 1990; Stewart, 1980; Stewart and Carlson, 1978; O'Leary, this volume). Its Quaternary history is characterized by high-angle left-lateral strike-slip faulting on several individual segments. (See O'Leary, this volume.) The RVFZ is one of several mapped generally northeast trending fault zones in the south-central NTS (Carr, 1984), including the Cane Spring, Wahmonie, and Mine Mountain systems (fig. 1). A notable increase in earthquake activity has occurred in the RVFZ since the LSM sequence, suggesting that the LSM event may be in some way related to strain in the RVFZ. This activity has included a sequence of several hundred earthquakes at unusually shallow depths in 1993 in addition to several other M 3.5+ events over the past several years. (See Smith, Shields, and Brune, this volume.) Figure 1 also shows earthquake activity from the SGBSN catalog from 1978 to just prior to the LSM earthquake. Except for those areas where underground nuclear testing took place, the highest concentrations of background seismicity on the NTS have been observed in and around western Rock Valley.

Acknowledgments

Wally Nicks, Austin Wilson, and Charlotte Middlebrooks maintained operations of the SGBSN at the University of Nevada-Reno through the Little Skull Mountain sequence. John Perry maintained the portable array through the end of 1992. Stephen Gillett assisted to a large degree in the processing and organizing of the large amount of portable data that was collected during the sequence. We also thank Steve Harmsen, Joan Gomberg, Edward Cranswick, Mark Meremonte, and Jim Brooks of the USGS for their help in the field deployment and for supplying their portable data.

Little Skull Mountain Mainshock

Table 1 summarizes the seismic moments and focal mechanisms for the mainshock from various sources. We determined an M_L of 5.8 (±0.2) from the UNRSL regional digital network (Savage and Anderson, 1995), and NEIC reported an M_L of 5.6. The short-period *P*-wave first-motion focal mechanism as well as an interpretation of the preferred fault plane based on the aftershock geometry is shown in figure 2. The focal mechanisms of the mainshock and the July 5 M 4.4 and September 13 M 4.5 aftershocks shown in figure 2 were determined using program FPFIT (Reasenberg and Oppenheimer, 1985).

The orientations of the fault planes of the mainshock mechanism are well constrained by Pn readings at regional distances (UNRSL northern Nevada seismic network). The preferred fault plane (dashed in fig. 2) dips steeply to the southeast and is selected based on the distribution and alignment of early aftershock activity (discussed following). The mainshock involved primarily normal displacement with a small left-slip component (T-axis: strike N.135°E., plunge 68°; P-axis: strike N.359°W., plunge 30°).

Meremonte and others (1995) have suggested that the LSM earthquake occurred on a southwestward extension of the Mine Mountain fault zone (MMFZ). This interpretation is based on the dip of the mainshock fault plane (16° shallower than the solution from this study) and the resulting alignment with the MMFZ. The strike of the Harmsen (1994) mechanism (the same focal mechanism referred to in Meremonte and others, 1995) is within the error estimate of the solution in this study, and the dip of the Harmsen solution is only 1° outside of the error bound (table 1). Extensions of the MMFZ through Jackass Flat are not supported by field data, and Quaternary activity along MMFZ is only documented along its northern part (Piety, 1996). For a dip of 70° and a hypocentral depth of 11.8 km, the LSM fault plane projects to the surface in southern Jackass Flat, south of mapped sections of the MMFZ (fig. 1). To associate the LSM event more confidently with the MMFZ, with the implication that the MMFZ shows Holocene activity and is

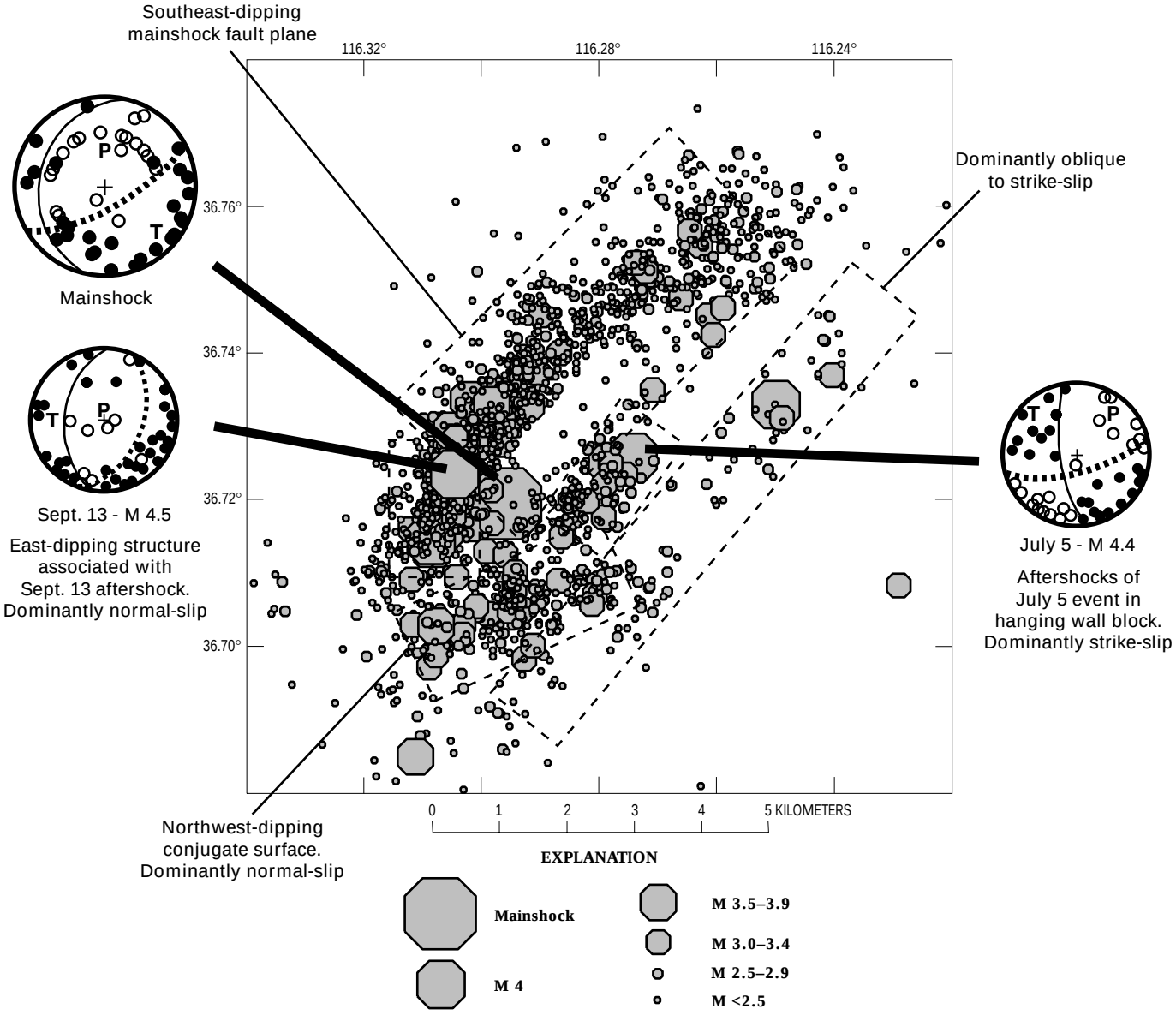

Figure 2. LSM earthquake activity, June–December 1992. Plotted are events that meet criteria for good location quality.

Table 1. Mainshock focal mechanisms and moment estimates. *

Source	Strike	Dip	Rake	M_o x 10^{24} dyne-cm
This study	60 ±15	70±13	–70±10	-
Meremonte and others (1995)	55	56	–72	-
Romanowicz and others (1993)	43	66	–73	3.5
Romanowicz and others (1993)	34	44	–70	2.6
Zhao and Helmberger (1994)	45	55	–60	3.0
Walter (1993)	35	54	–87	4.1
Harmsen (1994)	55	56	–72	-

* From John Schneider, written commun., 1995. -, no data.

nearly twice its current length, may require more detailed geologic and geophysical studies in southern Jackass Flat. Also, the orientation of the LSM fault plane, based on both the short-period focal mechanism and imaging of the early aftershock activity (discussed following), indicates an alignment intermediate between the strike of the RVFZ and the MMFZ. Although there is a general alignment of the LSM fault plane and the MMFZ to the north, the LSM event occurred where the MMFZ and the Cane Spring fault zone, Wahmonie fault zone, and RVFZ tend to intersect. This could as well be a zone of

complex deformation with intersecting faults of a variety of orientations not clearly associated with any one particular structure.

A 30-station strong-motion network was in operation in southern Nevada at the time of the LSM event (Lum and Honda, 1992). The closest station was 11 km southwest of LSM at Lathrop Wells, Nev. (SM#1; fig. 1). A peak acceleration of 0.206 *g* was recorded on the E.-W. component at this station (fig. 3). The second closest instrument, SM#2, was located 30 km northeast of the earthquake (peak acceleration of 0.150 *g*; fig. 3). The narrowing of the *S*-wave train at SM#2, relative to that observed for SM#1, is most likely due to rupture directivity along this source to receiver azimuth. The location of the mainshock hypocenter at the southwest extent of the aftershock zone (fig. 2) is consistent with unilateral

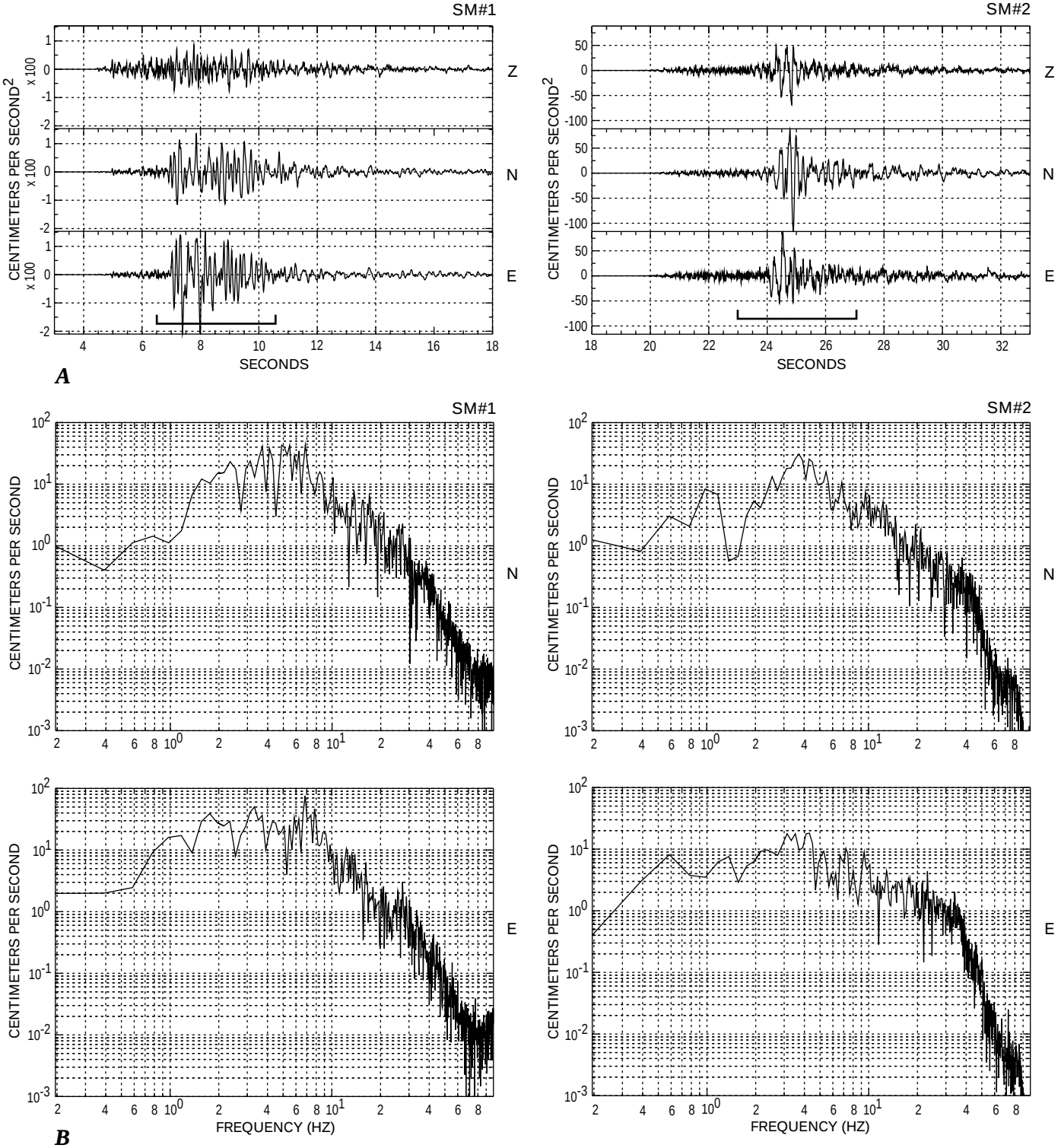

Figure 3. Acceleration time-series (*A*), and horizontal component *S*-wave acceleration spectra (*B*) of the LSM earthquake at strong-motion stations SM#1 and SM#2. Z, vertical component of ground acceleration; N, north-south horizontal component; E, east-west horizontal component. Brackets in *A* are intervals of time for which *S* –wave was sampled to calculate acceleration spectra in *B*.

rupture propagation to the northeast, toward SM#2. Figure 3 includes the *S*-wave acceleration spectra for both horizontal components of ground motion at SM#1 and SM#2, respectively. The highest accelerations were experienced in the 2–10 Hz band. The difference between the SM#1 and SM#2 spectra at high frequencies is most likely due to differences in the site conditions; SM#1 is located on a thick section of Quaternary alluvium and SM#2 is a hard rock site.

Earthquake Relocations and Focal Mechanism Determination

The LSM earthquake sequence occurred while the operation of the Southern Great Basin Seismic Network was in transition between the USGS in Golden, Colo., and the UNRSL. In addition, each group operated portable seismic instruments during the early part of the Little Skull Mountain sequence, and the UNRSL operated a portable array through December 1992. As a result, data used for the analysis of this sequence come from several sources covering various time periods. We have integrated the data sets to provide as much control as possible on aftershock locations and focal mechanisms.

Data

Data from the SGBSN, through October 1, 1992, were processed in Golden, Colo. (Harmsen, 1993). The USGS has published yearly Open-File Reports since 1978 on the operations of the SGBSN, which describe the recording scheme and hardware configuration of that system. Since September 1992, the UNRSL has operated the network, and the data are transmitted by microwave to the University of Nevada campus in Reno, Nev. In 1992, the accumulated data were digitized and processed through the CUSP processing software (Peppin and Nicks, 1992). At the time of the LSM earthquake, the SGBSN consisted of single-component vertical 1-Hz seismometers, with horizontal components at some stations. The network is operated at a high-gain in order to increase the magnitude detection threshold, but several horizontal components are operated at a lower gain to ensure on-scale horizontal component records for amplitude magnitude determinations (Harmsen, 1993; Gomberg, 1991).

The local magnitude (M_L) determined from a low-gain horizontal record at the near-source station on Little Skull Mountain (SGBSN station LSM) was assigned to earthquakes in the June through August time period (S.C. Harmsen, oral commun., 1992). Magnitudes from September through the end of 1992 were determined by the UNRSL using a duration magnitude scheme. During September 1992, both groups operated the SGBSN to provide some consistency in location and magnitude estimates through the transition period. UNRSL duration magnitudes, which were compared with USGS M_L measurements for the September time period, generally agree to within 0.1 magnitude units (D.H. von Seggern, UNRSL, oral commun., 1992), although some saturation of the coda magnitude estimate at low magnitudes has subsequently been observed.

Approximately 3,800 earthquakes were detected in the SGBSN during the LSM aftershock sequence from June through December 1992. On a few occasions, first-arrival times were determined from the optical backup records, due to down time in the data acquisition system. This was the case for the LSM mainshock, LSM foreshocks, and the first few hours of aftershock activity and other specific times reported by Meremonte and others (1993). Arrival times can be resolved to about 0.1 s (seconds) from optical records whereas accuracies of 0.01 to 0.02 s are typical for near-source 100-Hz digital recordings. Where necessary, first-motion readings from optical records have been included (S.C. Harmsen, oral commun., 1992).

Earthquake Relocation Procedure

Arrival times from the regional network and portable instruments were associated to create the first-arrival database. Earthquakes were located with program FASTHYPO (Herrmann, 1979) using the following variation of the one-dimensional velocity model of Hoffman and Mooney (1984) for the Yucca Mountain area.

Table 2. Velocity model.

Depth (km)	Velocity (km/s)
0	5.85
1	6
25	6.35
30	6.6
35	7.8

Hoffman and Mooney (1984) determined an average *P*-wave velocity of 3.0 km/s for a 1-km-thick surface layer. We have modified this to 5.85 km/s to account for larger *S*-wave travel-time residuals from near-source stations when using the slower surface velocities. This difference may be due to the high-velocity near-surface volcanic rocks at LSM. In order to develop a set of station corrections for network and portable instruments in the LSM area, only those events with more than 15 *P*-wave arrivals within 75 km of the aftershock zone were initially located. About 1,700 events with 25,000 individual phase arrival times were used. We chose 75 km as an arbitrary distance cutoff to minimize the problems associated with accurate timing of phases at regional distances and to minimize the contribution from travel paths through the deeper crust where we have less confidence in the velocities.

Average travel-time residuals were determined for each station from the suite of *P*-wave residuals with respect to the preceding one-dimensional velocity model. These average station residuals account, in a general way, for differences between the velocity model and the true three-dimensional velocity structure; they also incorporate local site corrections. The entire suite of earthquakes was relocated applying the average station residuals as station corrections. Station travel-time residuals and event root-mean-square (RMS) residuals for the set of relocated events decreased significantly following relocation (after

applying station corrections, RMS event residuals decreased an average of 0.15–0.08 s). Meremonte and others (1995) applied a similar method.

In order not to obscure the details of the aftershock distribution, only those earthquake locations that met particular, but reasonable, statistical location criteria are shown in the illustrations in this report. These constraints are an RMS residual of less than 0.1 s, a location gap of less than 120°, and 10 or more stations within 75 km epicentral distance used in the location. Absolute location errors are estimated to be less than 1 km in the horizontal dimension and less than 2 km in depth, although we believe that the relative location accuracy is within several hundred meters. These error estimates are based on the average RMS residuals. Focal mechanisms were determined for all events with more than 15 *P*-wave first-motion arrivals, and this resulted in 517 events that returned unique mechanism solutions (greater uncertainty can result in multiple solutions).

Aftershock Distribution, Mainshock Source Parameters, Focal Mechanism Distribution, and Foreshock Activity

Aftershock Distribution

Quality relocations of LSM aftershocks show faulting on several structures, with most aftershock activity confined to the mainshock fault plane. However, the majority of the moment release in the aftershock period was dominated by three M_L 4+ earthquakes, none of which occurred on the mainshock fault plane. Figure 2 is an epicentral map of all earthquake activity in the LSM area that followed the Landers earthquake through the end of December 1992. Only those events that met the criteria for good location quality previously described are included. The study area (dotted rectangle) in figure 1 is the area covered in figure 2. The mainshock is the large symbol at the southwest end of a northeast-trending elliptical area, in map view, that is generally free of aftershock activity. Three M_L 4+ events, the largest aftershocks, occurred during this time period. The first of these larger aftershocks occurred immediately following the mainshock, and its focal mechanism is poorly constrained. The M_L 4+ event of July 5 (0654 13.27 UT; fig. 2) occurred approximately 2 km northeast of, and 6 days after, the mainshock [lat 36°43.55′ N., long 116°16.46′ W.; depth 9.39 km; fault plane parameters: strike N.75° E., dip 70° E., rake –20°; T-axis: strike N. 30° E., plunge 89°; P-axis: strike N. 34° W., plunge 62°]. This event was followed by its own localized aftershock sequence confined to the hanging wall of the mainshock fault plane. The third M_L 4+ aftershock (September 13, 1146 20.87 UT) occurred within the dense cluster of activity less than 1 km west of the mainshock epicenter (fig. 2) [lat 36°43.41′ N., long 116°18.28′ W.; depth 8.93 km; fault plane parameters: strike N.20° E., dip 45° SE., rake –80°; T-axis: strike N.283° E., plunge 90°; P-axis: strike N.16° W., plunge 70°] .

Early Aftershock Activity—Mainshock Source Parameters

All major features of the aftershock distribution, except the strike-slip features associated with the July 5 M_L 4+ event, developed in the first 38 hours of the sequence (fig. 4). The cross section of figure 5 illustrates what we interpret to be the mainshock fault plane, striking N.48° E. and dipping 66° SE. This is a 12° counterclockwise direction to the orientation of the mainshock fault plane from the short-period mechanism, but inasmuch as the mechanism represents only the initiation of faulting, these estimates may not necessarily be identical. Because very few earthquakes were located at shallow depths, only the 5–13 km depth range is shown in figure 5. Moreover, shallowest events tended only to occur above the northeast end of the mainshock fault plane. Figure 6 is a projection showing that nearly all relocated hypocenters fall below a 5 km depth. Figure 6 includes all aftershock activity shown in figure 2, except that the hanging wall activity has been removed so as not to obscure the interpreted slip surface on the mainshock fault plane.

Figure 5 also shows the orientation of a fault surface that is conjugate to the mainshock fault plane. This structure dips approximately 45° NW. and is neither consistent with the orientation of the auxiliary fault plane of the mainshock mechanism nor aligned with the mainshock hypocenter. Therefore we do not see evidence that this is the mainshock fault plane. Isolating all structural features with cross-sectional views is difficult, but the focal mechanisms of this particular group of earthquakes suggest down-to-the-northwest normal motion on this minor feature (discussed following).

We interpret the semicircular distribution of early aftershock activity west, north, and northeast of the mainshock hypocenter to represent the upper boundary of the mainshock slip surface (figs. 2 and 6). Deeper events on this structure that plot within 3 km (epicentral distance) northeast of the mainshock, both in map view (fig. 2) and in perspective view (fig. 6), also appear to outline this area at depth. These deeper earthquakes were predominantly confined to the first 38 hours of the sequence, whereas aftershock activity defining the upper portion of the interpreted rupture surface continued throughout the sequence. The lack of aftershocks within this proposed slip area suggests nearly complete stress release on this fault surface during the earthquake.

The static stress drop and average slip during the mainshock can be estimated using an approximation of the geometry of the rupture surface and the M_o. The elliptical region in plan view in figure 4, and in projection in figure 6, roughly approximates a circular surface with a radius (r) of between 2.5 and 3.0 km. The stress drop ($\Delta\sigma$) for a circular fault (Brune, 1970; Aki and Richards, 1980) is given by

$$\Delta\sigma = \frac{7}{16}\ \frac{Mo}{r^3}$$

Static stress drops and average displacements for the Little Skull Mountain event are shown in table 3 for a range of source radii and published moments.

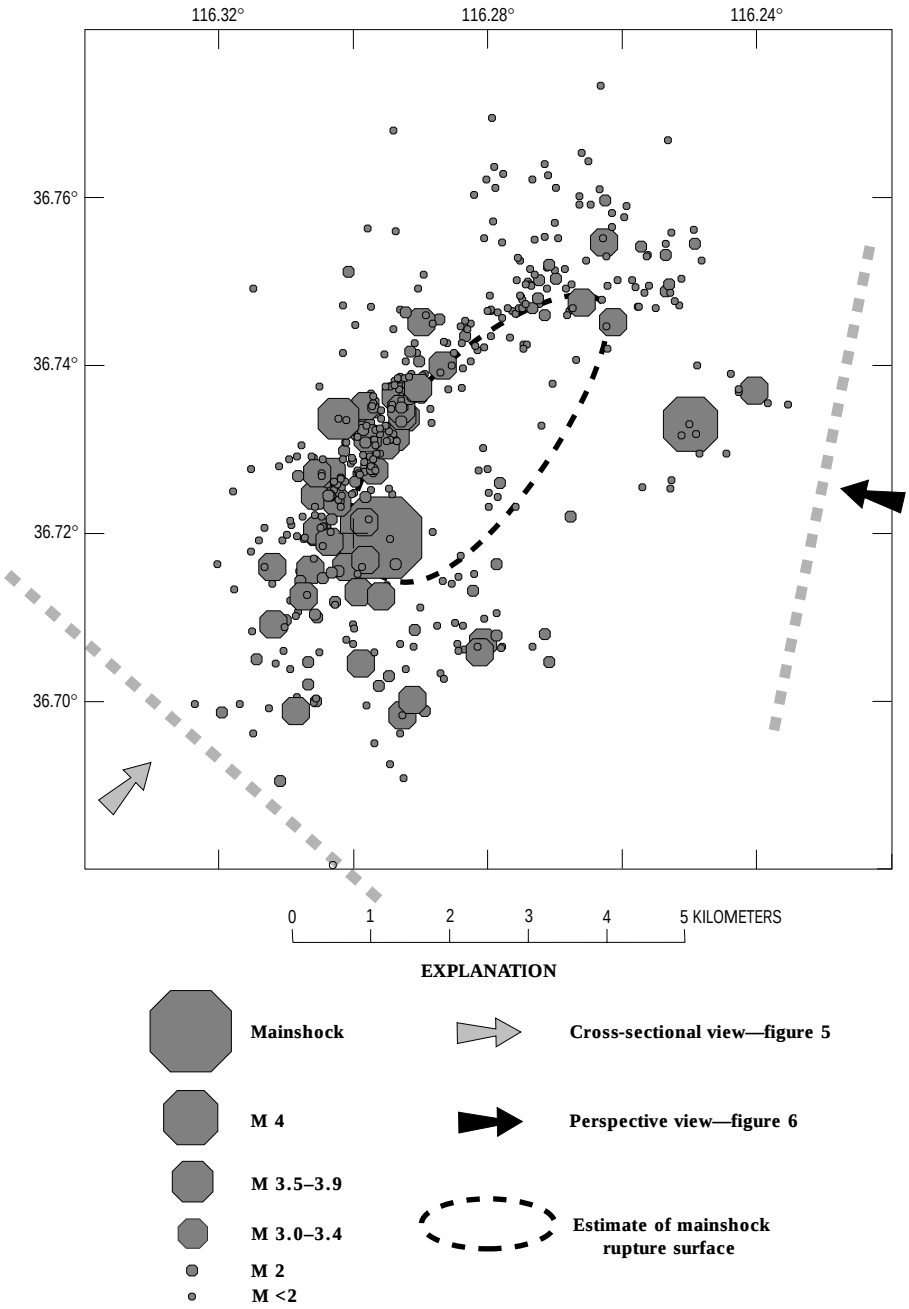

Figure 4. First 38 hours of aftershock activity (June 29-30, 1992).

Table 3. Mainshock source parameters.

Seismic moment (dyne-cm)	Reference	Source radius (km)	Stress drop (bars)	Fault slip (cm)
4.1×10^{24}	Walter (1993)	2.5	114	69
4.1×10^{24}	Walter (1993)	2.75	86	57
4.1×10^{24}	Walter (1993)	3	66	48
5.5×10^{24}	Harvard CMT	2.5	154	93
5.5×10^{24}	Harvard CMT	2.75	115	77
5.5×10^{24}	Harvard CMT	3	89	64

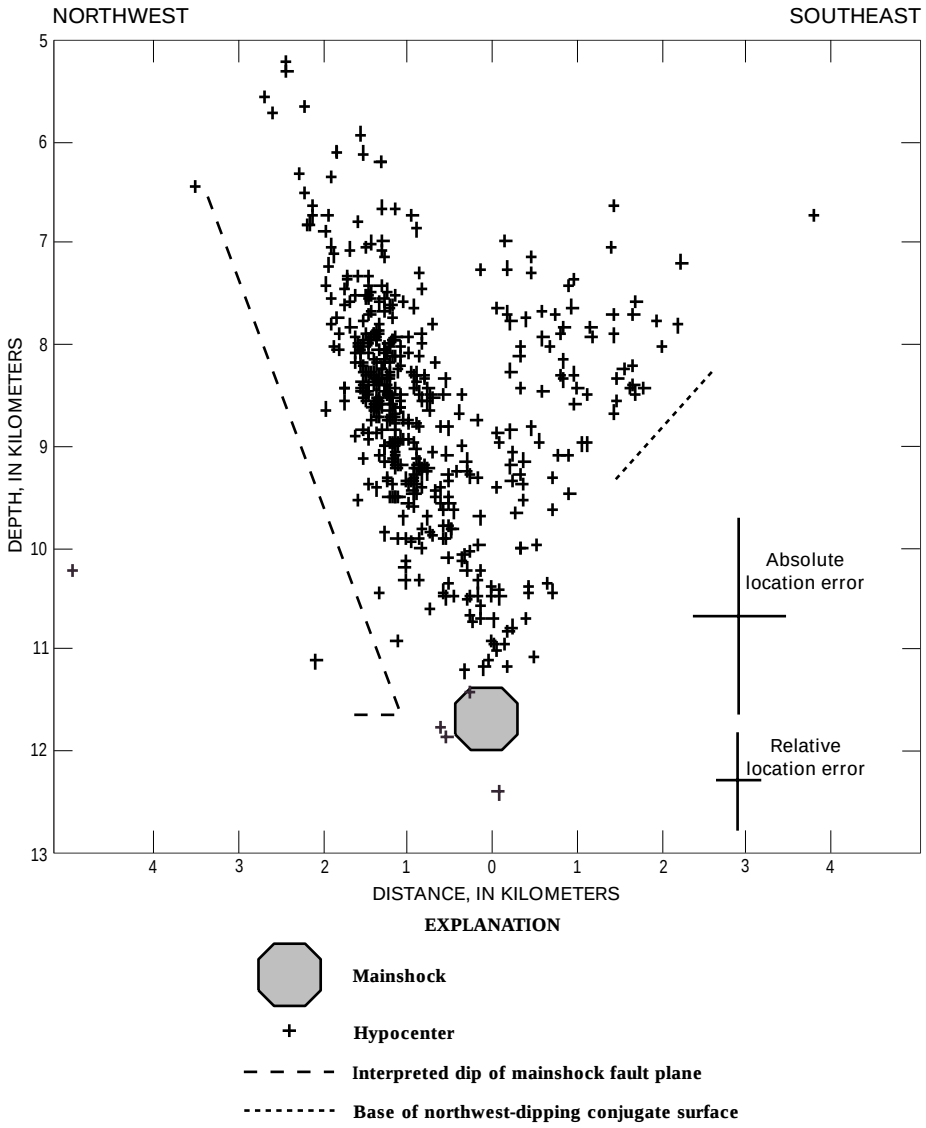

Figure 5. Cross section (29 June and 30 June) showing dip of mainshock fault plane and early "off-fault" aftershock activity in the depth range 5–13 km. View is N. 48° E.

A source radius of 2.5 km most closely approximates the area that is free of aftershock activity (figs. 4 and 6), whereas a 3 km radius includes most of the activity at the southwest and northeast ends of the aftershock zone. The interpreted rupture area in figures 4 and 6 may be better approximated by an ellipse rather than a circle, which would decrease our estimates of the rupture area and thereby increase the static stress drop estimate. These estimates are based on the assumption that the distribution of aftershocks is directly related to the extent of faulting during the main event. Walter and Mayeda (1996) calculated a stress drop of 196 bars for the LSM earthquake based on the radiated energy at regional stations. These static stress drop estimates are high compared to stress drop estimates for California earthquakes. A thorough analysis of the LSM source is being conducted in other Yucca Mountain studies and is beyond the scope of this report.

In the Basin and Range province, near-source studies of the source parameters of normal faulting events have been few. Boatwright (1985) determined the static stress drops of aftershocks of the Borah Peak earthquake, but no near-source waveforms were available for the mainshock. At Borah Peak, aftershock stress drops fell into two general ranges of 35 and 77 bars, depending on the location of the event within the aftershock zone. Ichinose and others (1997) estimated a stress drop of 60 bars for the magnitude 4.5 main event of the 1995 Border Town, Nev., sequence. Walter and Mayeda (1996) found no significant difference between the stress drops of normal and strike-slip events, but the data set for normal faulting events is limited. Clearly, understanding the unique aspects of the source processes for normal faulting events is important to understanding the seismic hazard in the extensional environment at Yucca Mountain.

The dense concentration of aftershocks west of the mainshock epicenter, which defines the western extent of the sequence (fig. 2), indicates a high level of activity in the early aftershock period (fig. 4). This area shows predominantly normal faulting (figs. 2, 7), defining an east-dipping structure that includes the September 13 event. Consistent with these focal

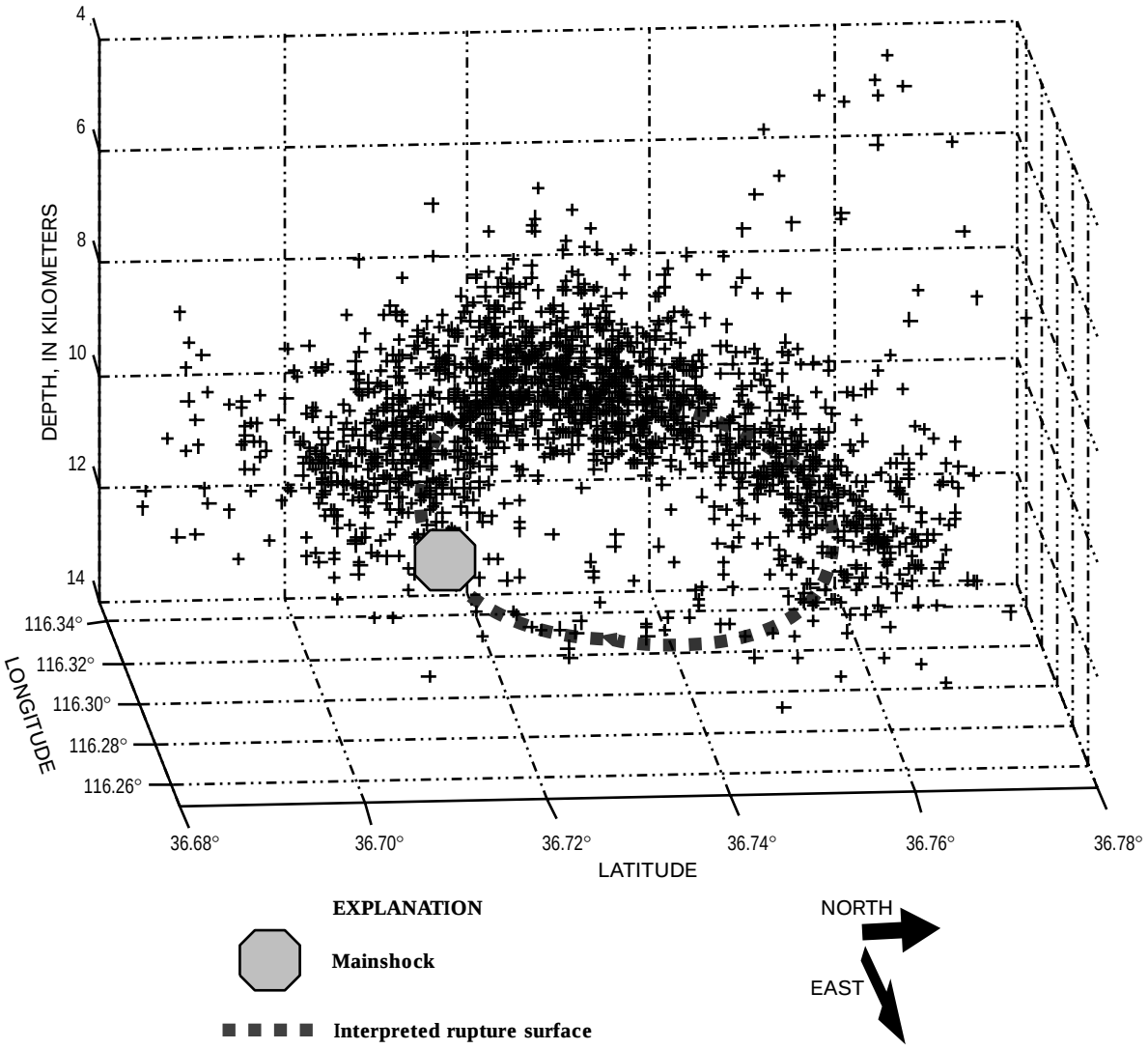

Figure 6. Perspective view of the mainshock fault surface. View is WNW., 10° above horizontal; +, hypocenter.

mechanisms, the trend in the aftershock distribution in this locality is generally north-south, in contrast to the northeast-striking trend of activity that conforms to the mainshock fault plane. This north-south-striking structure would intersect the mainshock fault plane at a high angle and would therefore limit or truncate its western extent. Although aftershocks of the September 13 M_L 4+ event dominate the later aftershock period, this north-south-striking structure was active at the M 3+ level immediately after the mainshock (fig. 4). In contrast to the east-dipping character of this fault surface, north-striking mid-Tertiary normal faults on Little Skull Mountain show a down-to-the-west geometry similar to that of faults in the central Yucca Mountain block (Frizzell and Shulters, 1990; Day and others, 1998).

The presence of the east-dipping structure just discussed suggests another interpretation for displacement during the LSM mainshock: coseismic slip occurred on this feature, causing down-to-the-northeast displacement of its hanging wall block and a similar displacement along the mainshock fault plane. The small component of left-slip in the mainshock focal mechanism (fig. 2) may be an expression of this faulting mechanism. This hypothesis may be difficult to test from regional records; slip on the east-dipping fault surface would exhibit a different focal mechanism than the mainshock, and the moment release on the subsidiary structure would be, at most, only 15–20 percent of that on the northeast-striking mainshock fault plane.

Activity that forms the southeastern extent of the aftershock distribution includes the June 29 M 4+ event and several other M 3+ earthquakes (figs. 2 and 4). In map view this activity extends between LSM and Skull Mountain and may represent reactivation of mapped mid-Tertiary faults or a southern extension of the Wahmonie fault zone. Activity along this northeast trend is dominated by strike-slip and oblique-slip focal mechanisms (fig. 7) and does not exhibit a wide depth distribution (fig. 5).

Focal Mechanism Distribution

Figure 7 summarizes the spatial distribution of 89 strike-slip and 198 normal-slip focal mechanisms; only those events with a T-axis inclination of less than 30° are plotted. In this

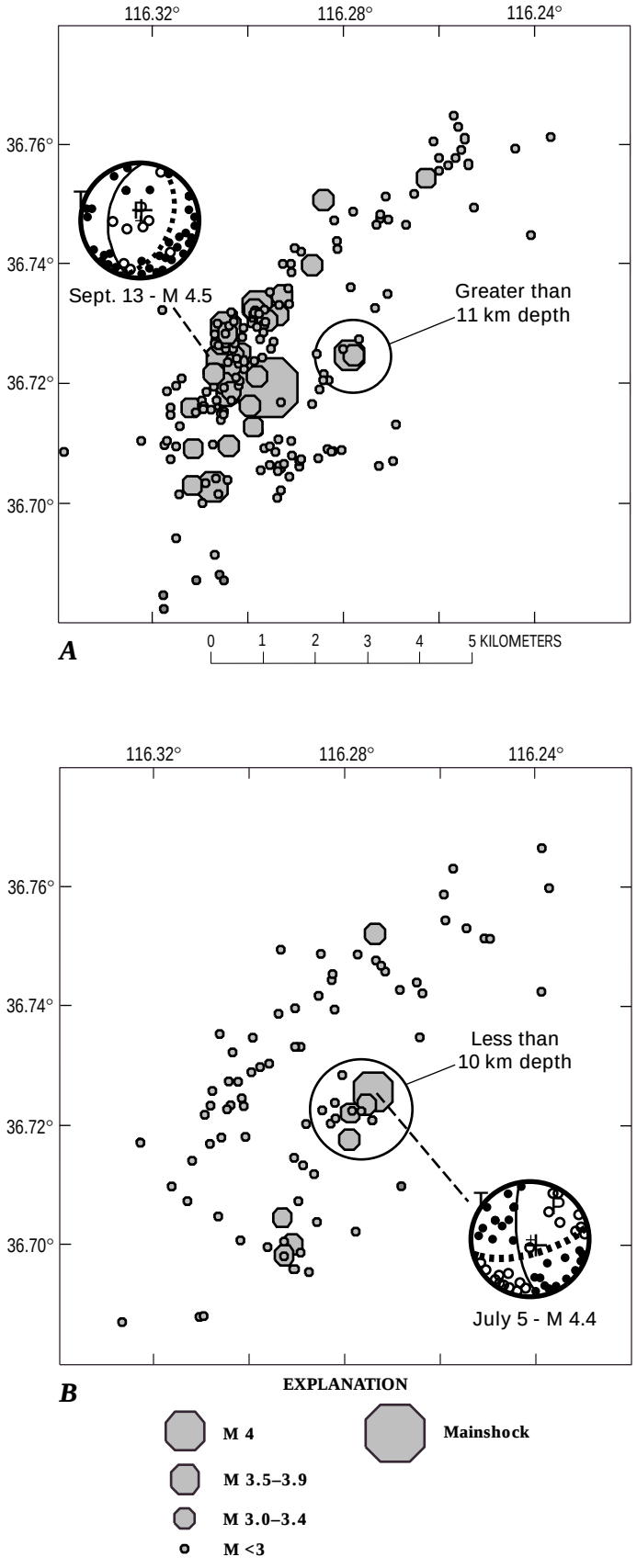

Figure 7. Spatial distribution of *A*, normal-slip and *B*, strike-slip short-period focal mechanisms.

figure, normal-slip events are defined as having a P-axis inclination of greater than 60° (higher angles represent a more vertically oriented stress axis). Strike-slip events are those with a P-axis inclination of less than 30°. Oblique-slip events are not included in order to isolate the normal- and strike-slip deformation. Only one M 3+ strike-slip event is associated with the mainshock fault plane, and this event is at the northeast end of the aftershock zone. M 3+ normal-slip aftershocks conform to the mainshock fault plane and the east-dipping structure associated with the September 13 M 4+ aftershock. Normal faulting events that occur south of the mainshock are associated with the generally north northwest dipping feature that appears to intersect the mainshock fault plane that was discussed previously with reference to the early aftershock period (figs. 2, 4, 5, and 7).

A cluster of strike-slip events associated with the July 5 M 4 earthquake trends generally northeast southwest (fig. 7*B*). The July 5 earthquake and its aftershock sequence lie above a depth of 10 km, and are confined to the hanging wall block of the mainshock fault plane. A group of normal faulting events in this same epicentral area occur below a depth of 11 km (fig. 7) and are at the base of the southeast-dipping mainshock fault plane (figs. 4 and 6). The preferred fault plane from the focal mechanism for the July 5 event and its aftershocks is therefore subparallel to the mainshock fault plane. Harmsen (1994) suggested that the July 5 earthquake is a right-slip event, but we prefer the northeast-striking fault plane because of the general northeast aftershock alignment.

Based on an alignment of north-northeast-oriented high-angle right-slip fault planes in the region of the July 5 earthquake, Harmsen (1994) and Meremonte and others (1995) suggested that some of this activity may be in the Wahmonie fault zone. We see little direct evidence for right-lateral strike-slip faulting in the LSM data. To support the argument for the sense-of-motion during the July 5 event and related aftershocks, we also point out that this structure is sub-parallel to the trend of the Rock Valley fault zone (fig. 1), a predominantly high angle left-slip structure. Activity on the structure associated with the July 5 event more clearly defines a northeast alignment by including aftershock data through the end of 1992.

Figure 8 shows lower hemisphere composite P and T diagrams from the 517 unique solution focal mechanisms covering the LSM sequence. The average azimuth of the T-axes is N. 62° W., and Harmsen (1994) reported an average T-axis direction of N. 60° W. These values are consistent with other studies of the orientation of the stress field in the southern Great Basin (Rogers and others, 1987; Harmsen and Bufe, 1992). The average T-axis orientation is rotated 20° counterclockwise with respect to the azimuth of the T-axis determined for the mainshock from this study. That a number of strike-slip events occurred can be deduced from the P-axis distribution, but normal-slip was the dominant sense of motion throughout the aftershock sequence. A few low-angle mechanisms in the LSM set, representing a small fraction of the total moment release, show no consistent spatial pattern similar to that shown by the strike-slip and normal-slip events and cannot be interpreted in terms of through-going low-angle structures. It is not unusual to observe some low-angle extensional or reverse-slip focal mechanisms in Basin and Range aftershock sequences.

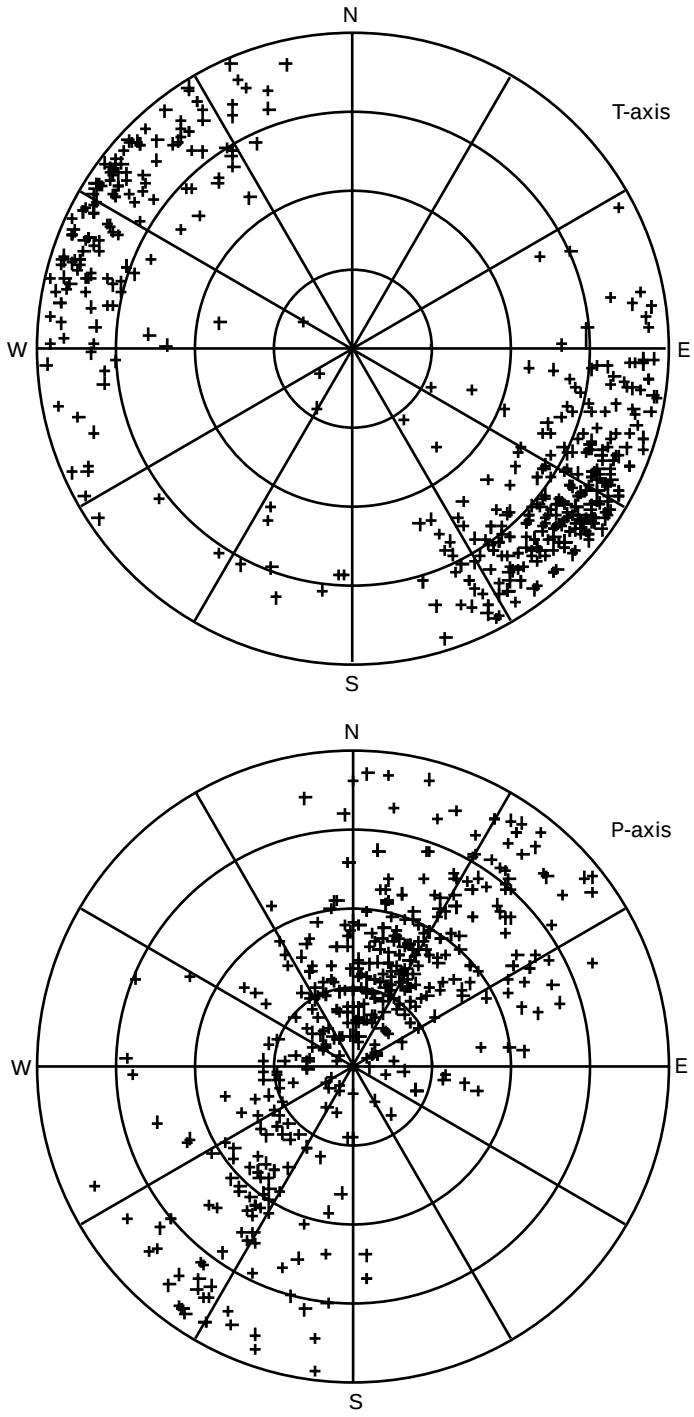

Figure 8. Lower hemisphere composite P- and T-stress axes distributions.

Foreshocks

The source region of the LSM earthquake was active immediately following the June 28, 1992, M_S 7.5 Landers, Calif., earthquake. A micro-earthquake array operating at Yucca Mountain (Brune and others, 1992), 20 km west of LSM, detected a marked increase in micro-earthquakes at LSM immediately following the Landers event (*S* minus *P* times were consistent with the distance to LSM for the entire set). On the basis of this evidence, Anderson and others (1994) and Gomberg and Bodin (1994) suggested that the Little Skull Mountain earthquake was dynamically triggered by surface waves generated by the Landers earthquake, although other physical processes for triggering of the LSM event have also been proposed (Bodin and Gomberg, 1994).

Figure 9 shows the cumulative number of events recorded on a high-gain seismograph station located near Yucca Mountain prior to the LSM mainshock. Twelve of these events, including one M 3+ event, could be located with SGBSN data within the coda of Landers aftershock activity (fig. 10). No micro-earthquake activity was observed on faults within the immediate vicinity of Yucca Mountain during the LSM foreshock period or LSM postseismic activity.

Summary and Conclusions

Although the Little Skull Mountain earthquake is a dominantly normal slip event, it does not conform to the classic range-front normal-faulting geometry that characterizes the Basin and Range province. In contrast to typical Basin and Range style normal-fault geometry, the hanging wall block, crest of LSM, is topographically higher than the footwall. Because no expression of Quaternary faulting has been recognized near the surface projection of the Little Skull Mountain mainshock fault plane in Jackass Flat, this particular structure has experienced very little displacement through Tertiary time. Several other recent moderate-sized earthquakes in the Basin and Range have not been associated with mapped faults and this observation is not unusual (for example: 1984 magnitude 5.8, Round Valley, Calif. (Priestley and others, 1988); 1986 magnitude 5.8 and magnitude 6.3 Chalfant, Calif. (Smith and Priestley, 1988); magnitude 6.0 1994 Double Spring Flat (data of Diane dePolo, 1994)).

Evidence for the steeply dipping geometry of the mainshock fault plane from well-located aftershocks and the short-period focal mechanism places the surface expression of the LSM earthquake southeast of that shown by Meremonte and others (1995). Based on a general alignment, they suggested that the LSM event may have occurred on a southwestern extension of the MMFZ. (See O'Leary, this volume.) Other than this geometry, there is little evidence to suggest that the MMFZ extends through the Jackass Flat basin. If this is a southern extension of the MMFZ, based on the observation that the hanging wall has greater relief than the footwall, then this section of the fault has very little cumulative offset.

From the geometry of the structures within the aftershock zone, the mainshock appears to have initiated at the intersection of the southeast-dipping mainshock rupture plane and a northeast-striking high-angle fault, possibly a southwest extension of the Wahmonie or even Cane Spring fault zones. This is also implied by Meremonte and others (1995). Mapped expressions of the Mine Mountain, Wahmonie, and Cane Spring all trend into the RVFZ in the LSM source region, and isolating one of these faults in the LSM area may be problematic. This area may be a focal point for increased stress concentration, as illustrated by the concentration of pre-LSM seismicity (fig. 1), which may indeed be the consequence of the interaction of

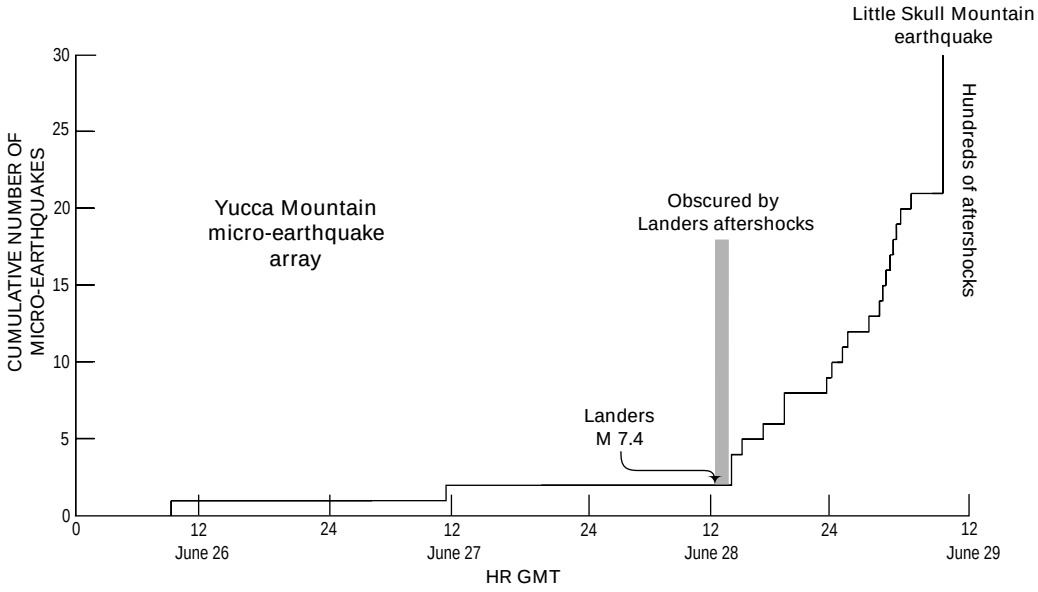

Figure 9. Cumulative microseismic activity from LSM source region prior to mainshock event.

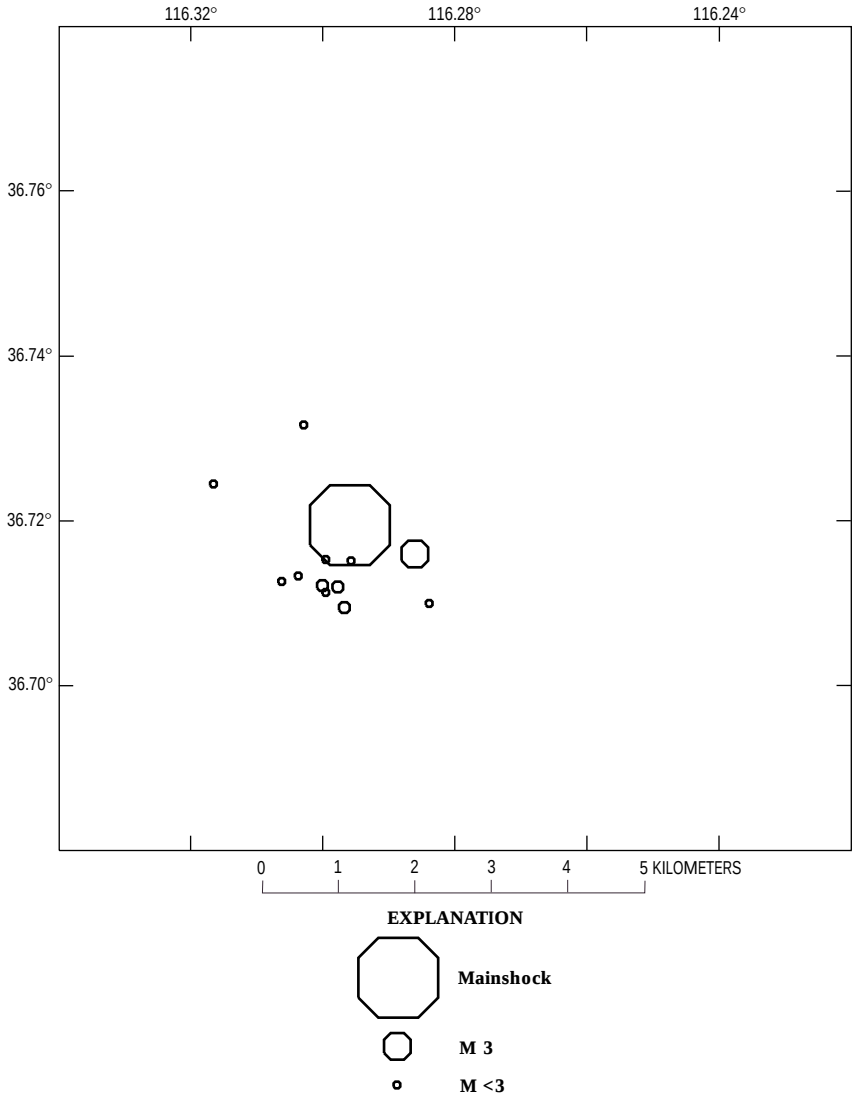

Figure 10. Location of LSM foreshock activity in hours following Landers earthquake.

these south-central NTS structures. Because the RVFZ is the most active of these structures, a reasonable proposal is that the LSM event may have been influenced by deformation associated with the RVFZ rather than the MMFZ.

No M 4+ LSM aftershocks took place on the mainshock fault plane, but such events occurred on subsidiary structures within the aftershock zone. A set of aftershocks directly west of the mainshock epicenter aligns along a distinct northerly trend. This alignment is consistent with the normal-slip focal mechanism of the September 13 M_L 4+ event and a number of normal-slip aftershocks. The preferred fault plane for the M 4+ September 13 event strikes nearly north south and dips to the east. Near the epicenter of the latter event, the aftershock distribution defines an intersection between the southeast-dipping mainshock fault plane and this east-dipping structure. This is also the location of LSM foreshock activity and the point of initiation of mainshock rupture.

The time of initiation of foreshock activity suggests that the LSM earthquake was triggered by surface wave energy generated during the June 28 Landers, Calif., event (Anderson and others, 1994). Micro-earthquake activity in the LSM source region was observed immediately following the Landers event, and foreshock activity continued to the time of the LSM mainshock. Because of close proximity to Yucca Mountain, the LSM earthquake and aftershock sequence have been particularly important for ongoing seismic hazard studies.

References Cited

Aki, K., and Richards, P., 1980, Quantitative seismology—Theory and methods: San Francisco, W.H. Freeman.

Anderson, J.G., Brune, J.N., dePolo, Diane, Gomberg, Joan, Harmsen, S.C., Savage, M.K., Sheehan, A.K., and Smith, K.D., 1993, Preliminary report—The Little Skull Mountain earthquake, June 29, 1992, *in* Dynamic analysis and design considerations for high-level nuclear waste repositories: Structural Division/American Society of Civil Engineers, p. 162–175.

Anderson, J.G., Brune, J.N., Louie, J.N., Zeng, Y., Savage, M.K., Yu, G., Chen, Q., and dePolo, D., 1994, Seismicity triggered by the Landers, California, Earthquake, 28 June 1992: Bulletin of the Seismological Society of America, v. 84, p. 863–891.

Boatwright, J., 1985, Characteristics of the aftershock sequence of the Borah Peak, Idaho, earthquake determined from digital recordings of the event: Bulletin of the Seismological Society of America, v. 75, p. 1265–1284.

Bodin, P., and Gomberg, J., 1994, Triggered seismicity and deformation between the Landers, California, and Little Skull Mountain, Nevada, earthquake: Bulletin of the Seismological Society of America, v. 84, p. 835–843.

Brune, J.N., 1970, Tectonic stress and the spectra of seismic shear waves from earthquakes: Journal of Geophysical Research, v. 75, p. 4997–5009.

Brune, J.N., Nicks, W., and Aburto, A., 1992, Microearthquakes at Yucca Mountain, Nevada: Bulletin of the Seismological Society of America, v. 82, p. 164–174.

Carr, W.J., 1984, Regional structural setting of Yucca Mountain, southwestern Nevada, and late Cenozoic rates of tectonic activity in part of the southwestern Great Basin, Nevada and California: U.S. Geological Survey Open-File Report 84-854, 109 p.

———1990, Styles of extension in the Nevada Test Site region, southern Walker Lane Belt; An integration of volcano-tectonic and detachment fault models, *in* Wernicke, B.P., ed., Basin and Range extensional tectonics near the latitude of Las Vegas, Nevada: Geological Society of America Memoir 176, p. 283–303.

Day, W.C., Potter, C.J., Sweetkind, D.S., Dickerson, R.P., and San Juan, C.A., 1998, Bedrock geologic map of the central block area, Yucca Mountain, Nye County, Nevada: U.S. Geological Survey Miscellaneous Investigations Series Map I-2601, scale 1:6,000.

Dokka, R.K., and Travis, C.J., 1990, Role of the Eastern California shear zone in accommodating Pacific–North American plate motion: Geophysical Research Letters, v. 17, p. 1323–1326.

Fridrich, C.J., 1999, Tectonic evolution of the Crater Flat basin, Yucca Mountain region, Nevada, *in* Wright, L.A., and Troxel, B.W., eds., Cenozoic basins of the Death Valley region: Geological Society of America Special Paper 333, p. 169–175.

Frizzell, Jr., V.A., and Shulters, J., 1990, Geologic map of the Nevada Test Site, southern Nevada: U.S. Geological Survey Miscellaneous Investigations Series Map I-2046.

Gomberg, Joan, 1991, Seismicity and detection/location threshold in the Southern Great Basin Seismic Network: Journal of Geophysical Research, v. 96, p. 16401–16414.

Gomberg, Joan, and Bodin, P., 1994, Triggering of the M_S = 5.4 Little Skull Mountain, Nevada, earthquake with dynamic strains: Bulletin of the Seismological Society of America, v. 84, p. 844–853.

Harmsen, S.C., 1993, Seismicity and focal mechanisms for the southern Great Basin of Nevada and California in 1991: U. S. Geological Survey Open-File Report 92-340.

———1994, The Little Skull Mountain, Nevada, earthquake of June 29, 1992; aftershock focal mechanisms and tectonic stress field implications: Bulletin of the Seismological Society of America, v. 84, p. 1484–1505.

Harmsen, S.C., and Bufe, C.G., 1992, Seismicity and focal mechanisms for the southern Great Basin of Nevada and California; 1987 through 1989: U.S. Geological Survey Open-File Report 91-572.

Hauksson, E., Hutton, K., Kanamori, H., Jones, L., Mori, J., Hough, S., and Roquemore, G., 1995, Preliminary report on the 1995 Ridgecrest earthquake sequence in eastern California: Seismological Research Letters, v. 66, p. 54–60.

Herrmann, R.B., 1979, FASTHYPO—A hypocenter location program: Earthquake Notes, v. 50, p. 25–37.

Hill D.P., Reasenberg, R.A., Michael, A., Arabaz, W.J., Beroza, G., Brumbaugh, D., Brune, J.N., Castro, R., Davis, S., dePolo, Diane, Ellsworth, W.L., Gomberg, Joan, Harmsen, S.C., House, L., Jackson, S.M., Johnston, M.J.S., Jones, L., Keller, R., Malone, S., Munguia, L., Nava, S., Pechmann, J.C., Sanford, A., Simpson, R.W., Smith, R.B., Stark, M., Stickney, M., Vidal, A., Walter, S., Wong, W., and Zollweg, J., 1993, Seismicity remotely triggered by the magnitude 7.3 Landers, California, earthquake: Science, v. 260, p. 1617–1623.

Hoffman, L.R., and Mooney, W.D., 1984, A seismic study of Yucca Mountain and vicinity, southern Nevada; Data report and preliminary results: U.S. Geological Survey Open-File Report 83-588.

Ichinose, G., Smith, K.D., and Anderson, J.G., 1997, Source parameters of the 1995 Border Town, Nevada, earthquake sequence: Bulletin of the Seismological Society of America, v. 83, p. 652–667.

Lum, P.K., and Honda, K.K., 1992, Processed seismic motion records from Little Skull Mountain, Nevada, earthquake of June 29, 1992,

recorded at stations in southern Nevada: National Technical Information Service, Report # JAB-10733-TM6 UC-703.

Meremonte, M.E., Cranswick, Edward, Gomberg, Joan, Worley, D., Carver, D., Brooks, J., Banfill, R., Overturf, D., and Bice, T., 1993, Report on the seismological field investigations of the 29 June 1992 Little Skull Mountain earthquake: U.S. Geological Survey Open-File Report 93-555.

Meremonte, M.E., Gomberg, Joan, and Cranswick, Edward, 1995, Constraints on the 29 June 1992 Little Skull Mountain sequence provided by robust hypocentral estimates: Bulletin of the Seismological Society of America, v. 85, p. 1039–1049.

Meremonte, M.E., and Rogers, A.M., 1987, Historical catalog of southern Great Basin earthquakes 1868-1978: U.S. Geological Survey Open-File Report 87-80.

Peltzer, G., and Rosen, P., 1995, Surface displacement of the May 17, 1993 Eureka Valley California earthquake observed by SAR interferometry: Science, v. 268, p. 1333–1336.

Peppin, W.A., and Nicks, W.F., 1992, Real time analog and digital data acquisition through CUSP: Seismological Research Letters, v. 63, p. 181–189.

Piety, L.A., 1996, Compilation of known or suspected Quaternary faults within 100 km of Yucca Mountain, Nevada and California: U.S. Geological Survey Open-File Report 94-112.

Priestley, K.F., Smith, K.D., and Cockerham, R.S., 1988, The 1984 Round Valley, California earthquake sequence: Geophysical Journal, v. 95, p. 215–235.

Reasenberg, P.A., and Oppenheimer, D., 1985, FPFIT, FPPLOT, and FPPAGE; Fortran computerprograms for calculating and displaying earthquake fault-plane solutions: U.S. Geological Survey Open File Report 85-739.

Rogers, A.M., Harmsen, S.C., Corbett, E.J., Priestly, K.F. and dePolo, Diane, 1991, The seismicity of Nevada and some adjacent parts of the Great Basin, *in* Slemmons, D.B., Engdahl, E.R., Zoback. M.D., and Blackwell, D.D., eds., Neotectonics of North America: Geological Society of America, Decade of North American Geology, Map Volume 1, p. 153–184.

Rogers, A.M., Harmsen, S.C., and Meremonte, M.E., 1987, Evaluation of the seismicity of the southern Great Basin and its relationship to the tectonic framework of the region: U.S. Geological Survey Open-File Report 87-408.

Romanowicz, B., Dreger, Pasyanos, M., and Uhrhammer, R., 1993, Monitoring strain release in the central and northern California using broadband data: Geophysical Research Letters v. 20, p. 1643–1646.

Savage, M.K., and Anderson, J.G., 1995, A local magnitude scale for the western Great Basin-eastern Sierra Nevada from synthetic Wood-Anderson seismograms: Bulletin of the Seismological Society of America, v. 85, p. 1236–1245.

Schweichert, R.A., 1989, Evidence for a concealed strike-slip fault beneath Crater Flat, Nevada: Geological Society of America Abstracts with Programs, v. 21, p. A90.

Scott, R.B., 1990, Tectonic setting of Yucca Mountain, southwest Nevada, *in* Wernicke, B.P., ed., Basin and Range extensional tectonics near the latitude of Las Vegas, Nevada: Geological Society of America Memoir 176, p. 251–282.

Smith, K.D., and Priestley, K.F., 1988, The foreshock sequence of the 1986 Chalfant, California earthquake: Bulletin of the Seismological Society of America, v. 78, p. 172–187.

Stewart, J.H., 1980, Geology of Nevada: Nevada Bureau of Mines and Geology Special Publication 4.

Stewart, J.H., and Carlson, J.E., 1978, Geologic map of Nevada: Nevada Bureau of Mines and Geology Special Publication 4 supplement, scale 1:500,000.

Walter, W.R., 1993, Source parameters of the June 29, 1992 Little Skull Mountain Earthquake from complete regional waveforms at a single station: Geophysical Research Letters, v. 20, p. 403–406.

Walter, W.R., and Mayeda, K., 1996, Moment, energy, stress drop, and source spectra of western United States earthquakes from regional coda envelopes: Journal of Geophysical Research, v. 101, p. 11195–11208.

Zhao, L.S., and Helmberger, D.V., 1994, Source estimation from broadband regional seismograms: Bulletin of the Seismological Society of America, v. 84, p. 91–104.